AGU PUBLICATIONS

Geochemistry, Geophysics, Geosystems

RESEARCH ARTICLE
10.1002/2016GC006607

Special Section:
Magnetism From Atomic to Planetary Scales: Physical Principles and Interdisciplinary Applications in Geo- and Planetary Sciences

Effects of titanomagnetite reordering processes on thermal demagnetization and paleointensity experiments

Julie A. Bowles[1] and Mike J. Jackson[2]

[1]Department of Geosciences, University of Wisconsin – Milwaukee, Milwaukee, Wisconsin, USA, [2]Institute for Rock Magnetism, University of Minnesota, Minneapolis, Minnesota, USA

Abstract Titanomagnetite ($Fe_{3-x}Ti_xO_4$, $0 \leq x \leq 1$) is a common, naturally occurring magnetic mineral critical to many paleomagnetic studies. Underlying most interpretations is the assumption that, lacking chemical alteration, Curie temperature (T_c) remains constant. However, recent work has demonstrated that T_c of many natural titanomagnetites varies strongly as a function of thermal history, independent of chemical alteration. This is inferred to arise from reordering of cations and/or vacancies in the crystal structure, and changes occur at temperatures and times relevant to standard paleomagnetic thermal treatments. Because changes take place at $T < T_c$, they have the potential to dramatically affect thermal remanence acquisition or demagnetization, impacting interpretation of paleomagnetic results. Here we have modeled the effects of reordering on standard thermal demagnetization and paleointensity experiments. Results suggest that T_c changes during laboratory heating make it impossible to accurately measure the unblocking temperature spectrum without modifying it. Samples with a starting T_{c0} less than the closure temperature (T_{close}) for the reordering process will develop a high-temperature "tail" that did not exist prior to heating. Samples with a starting $T_{c0} > T_{close}$ will have their original T_b spectrum truncated at $T \approx T_{close}$. Predicted behavior during Thellier-type paleointensity experiments results in only modest deviations in NRM-lost or pTRM*-gained from the nonreordering case. Much larger deviations are predicted for pTRM checks. Compared to paleointensity results from titanomagnetite-bearing pyroclastic deposits, modeled nonideal behavior occurs in the same temperature intervals, but is much more systematic. Reordering is likely one contributing factor to failure of paleointensity experiments.

Key Points:
- Inferred cation reordering in titanomagnetite can affect paleomagnetic interpretations
- Cation reordering in titanomagnetite makes it impossible to accurately measure the unblocking temperature spectrum without modifying it
- Inferred cation reordering in titanomagnetite can result in apparent pTRM-check failure in paleointensity experiments

Supporting Information:
- Supporting Information S1

Correspondence to:
J. A. Bowles,
bowlesj@uwm.edu

Citation:
Bowles, J. A., and M. J. Jackson (2016), Effects of titanomagnetite reordering processes on thermal demagnetization and paleointensity experiments, *Geochem. Geophys. Geosyst.*, *17*, 4848–4858, doi:10.1002/2016GC006607.

Received 25 AUG 2016
Accepted 12 NOV 2016
Accepted article online 01 DEC 2016
Published online 17 DEC 2016

1. Introduction

Recent work has demonstrated that the Curie temperature (T_c) of many natural titanomagnetites ($Fe_{3-x}Ti_xO_4$, $0 \leq x \leq 1$) of intermediate composition (x between approximately 0.2 – 0.5) is a strong function of prior thermal history. These T_c variations seemingly arise from a reversible ordering or disordering of cations and/or vacancies in the cubic lattice structure, and T_c may vary by up to 150°C with no attendant change in mineral composition [*Bowles et al.*, 2013]. Significant changes in ordering occur at moderate temperatures (300–500°C) and on relatively short timescales (hours to months) relevant to both geological processes and standard paleomagnetic laboratory treatments.

This phenomenon has now been documented in historical pyroclastic deposits from Mt. St. Helens (Washington State), Novarupta (Alaska), Lascar (Chile), and Soufrière Hills (Montserrat); historical extrusive basaltic lava flows from Fogo; ~15 Ma Columbia River basalt feeder dikes; the 1100 Ma Duluth intrusive complex; and synthetic titanomagnetites [*Jackson and Bowles*, 2013, 2014; *Lappe et al.*, 2014]. All these samples contain titanomagnetite with moderate amounts of titanium substitution (x approximately 0.2 – 0.5) and frequently with small amounts of additional Mg and Al substitution.

If changes in T_c can occur over laboratory time scales of hours, we might expect this to influence results of laboratory thermal demagnetization or paleointensity experiments. For example, it is conceivable that the unblocking temperature spectrum of a natural remanence can be significantly altered by the very act of measuring it. To assess potential complications arising from this reordering behavior in remanence acquisition and demagnetization, we have modeled thermal demagnetization and paleointensity experiments, taking observed variations in T_c with thermal history into account. We utilize experimental data documenting

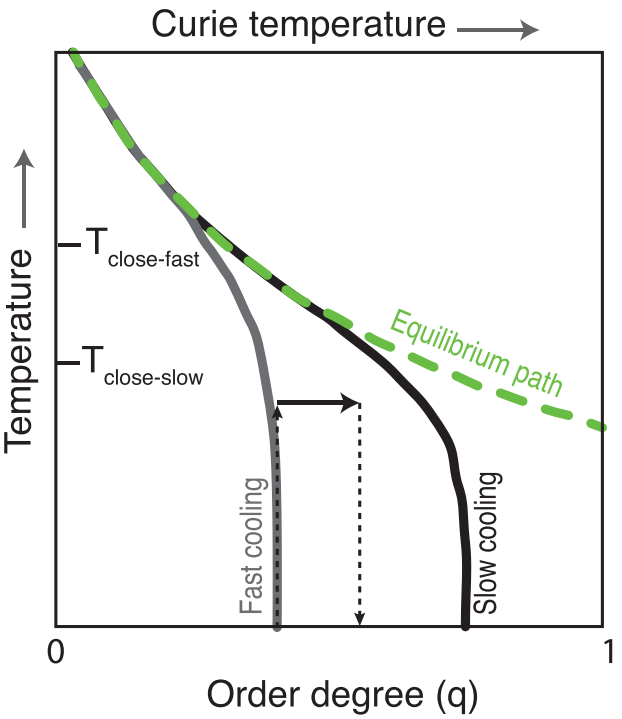

Figure 1. Schematic representation of a reordering process. The equilibrium order degree (and Curie temperature) increases with decreasing temperature (green dashed line). A rapidly cooled sample departs from the equilibrium path at a higher closure temperature ($T_{close\text{-}fast}$), quenching in a relatively low degree of order (and low T_c). Such a quenched sample may be driven toward equilibrium by annealing at elevated temperature, represented here by the light black dashed and solid arrows. Figure after *Bowles et al*. [2013].

the time-temperature evolution of T_c and apply it to remanence behavior using both single-domain Néel theory [*Néel*, 1949], as well as phenomenological models of multidomain behavior [*Fabian*, 2000].

2. The Reordering Process

The underlying physical process responsible for the T_c variations is inferred to be a reversible ordering or disordering of cations and/or vacancies in the cubic lattice structure [*Bowles et al*., 2013; *Jackson and Bowles*, 2014]. Although the precise reordering mechanism remains elusive, several lines of evidence suggest intra-site, as opposed to inter-site, reordering. This evidence includes lack of variations in M_s and lack of evidence for inter-site Fe^{2+}/Fe^{3+} exchange as measured by X-ray magnetic circular dichroism and Mössbauer spectroscopy [*Bowles et al*., 2013; *Lappe et al*., 2015]. This distinguishes the process from that documented for magnesioferrite ($MgFe_2O_4$) or the magnetite (Fe_3O_4)-spinel ($MgAl_2O_4$) solid solution, where inter-site reordering of magnetic cations results in variations in saturation magnetization (M_s), as well as a linear relationship between order degree and T_c [*Harrison and Putnis*, 1999]. In these latter cases, a spinel-structured oxide with only two cations can be written as $A_{1-y}B_y[A_yB_{2-y}]O_4$, where the inversion parameter y ranges from 0 (normal spinel) through 2/3 (disordered) to 1 (inverse spinel). The degree of order is parameterized in terms of the fraction of B cations in tetrahedral and octahedral coordination and is represented by an order parameter $Q=1\text{-}3y/2$. Q varies from 0 (disordered) to 1 (fully ordered normal spinel) or -0.5 (fully ordered inverse spinel).

In the observed natural titanomagnetite system, the presence of multiple impurities (Mg, Al, Ti) as well as a process dominated by intra-site reordering means that order degree is not so simply defined. Without specifying the exact nature of the order, and assuming a linear relationship between order degree and T_c, we define an order parameter, $0 < q < 1$, in terms of the observed T_c variations such that $q\ (T_c) = (T_c\text{-}T_{c,min})/(T_{c,max}\text{-}T_{c,min})$, where $T_{c,min}$ is the minimum T_c associated with the least ordered state ($q = 0$) and $T_{c,max}$ is the maximum T_c associated with the most ordered state ($q = 1$).

The measured T_c or order degree results from an interplay of two effects: an equilibrium degree of order $q_{eq}(T)$ that varies inversely with temperature (Figure 1), and reordering rates which vary directly with T. A low degree of order may be preserved at room temperature by rapid quenching, and a closure temperature (T_{close}) can be defined as the temperature at which a given cation distribution was last in equilibrium. Closure temperature is rate-dependent, and throughout this paper we define it with respect to rapid cooling over a few tens of minutes. By annealing an unequilibrated disordered sample at $T < T_{close}$, it moves toward the equilibrium state of higher q, and T_c increases accordingly (Figure 1).

Our modeling approach uses the results of such isothermal annealing experiments designed to document the time-temperature evolution of T_c in the titanomagnetite system. Results are presented in *Bowles et al*. [2013] and *Jackson and Bowles* [2014] but can be summarized as follows. Starting with a rapidly cooled, disordered sample (small q), there is a linear relationship between the logarithm of anneal time and T_c (supporting information Figure S1a), and the slope of this line is at a maximum for temperatures near ~375°C

(supporting information Figure S1b). Annealing at higher temperatures results in a decrease in activation time for the process, shifting the line to the left on a plot of T_c versus log (anneal time). The exact time-temperature relationship is composition-dependent, and for this work we use data from the May 18, 1980 Mt. St. Helens eruption (supporting information Figure S1), which has a composition of $Fe_{2.55}Ti_{0.26}Mg_{0.10}Al_{0.08}Mn_{0.01}O_4$. A cooling-rate-dependent closure temperature for the process is between 450 and 500°C, meaning that for samples cooled rapidly from above this temperature, the relatively disordered equilibrium cation distribution at $T_{close} \sim 475$°C will be quenched in. This corresponds to a Curie temperature of ~375°C.

3. Modeling

We take two approaches to the modeling, both of which allow blocking temperatures to vary proportionately with T_c. To simulate single-domain samples we use Néel theory, and for multidomain samples, we use a phenomenological approach [*Fabian*, 2000, 2001; *Leonhardt et al.*, 2004]. In both cases, starting T_c is allowed to vary between 375°C (representing a rapidly cooled sample) and 525°C (representing a slowly cooled or annealed sample). T_c evolves during the laboratory thermal treatments as described above, and we approach this numerically in the following way. At the start of each thermal treatment of temperature T_i and duration t_i, the sample has the Curie temperature from the previous treatment, Tc_{i-1}. The rate of change in T_c varies as it approaches equilibrium, but the information we have is simply the length of time required to produce a given Curie temperature from the disordered or quenched state (supporting information Figure S1a). Therefore, we first find how long it would take to achieve Tc_{i-1} at T_i if the sample had started in the quenched or disordered state. This time is added to the treatment duration and the total time is then used to find the new Tc_i. The closure temperature is 475°C, so anytime the sample is cooled from $T > T_{close}$, T_c reverts to 375°C.

We use the saturation magnetization formulation of *Dunlop and Özdemir* [1997], modified to account for the dependence on q:

$$M_S(T,q) = M_{S0}[1 - T/T_C(q)]^{\gamma}$$

Although *Dunlop and Özdemir* [1997] suggest a value of $\gamma = 0.43$ for magnetite, we use $\gamma = 0.39$, which *Tauxe* [2010] shows is a better fit to the available experimental data. Our data show that M_s at 10 K is independent of q [*Bowles et al.*, 2013]. Because T_c varies with q, M_s also must be a function of q, but in our models the saturation magnetization scales in the same way for all q as a function of reduced temperature, $M_s(T/T_c(q))$ (supporting information Figure S2). We recognize that the shape of the characteristic function $\chi(T_b,T_{ub})$ (defined below) may change with q if exchange coupling, anisotropy or magnetostriction constants also vary with q. These parameters may also affect remanence acquisition or demagnetization via effects on domain state or coercivity, but in the absence of any information on how they might vary with q, we assume the dependence is negligible.

In the SD case, we assume that (un)blocking temperature variations arise from a volume distribution, and blocking temperatures vary linearly between some $T_{b\text{-}min}$ (allowed to vary between simulations) and 375°C (T_c achieved on quenching from above T_{close}). We use the following relationship between blocking temperature and volume [*Dunlop and Özdemir*, 1997, equation (8.19)]:

$$\frac{T_b}{\vartheta^2(T_b)} = \left[\frac{\mu_0\ V\ M_{S0}H_{K0}}{2\ k\ \ln\left(\frac{t}{\tau_0}\right)}\right]\left[1 - \frac{|H_0|}{H_{K0}\vartheta(T_B)}\right]^2 \quad (1)$$

where T_b is blocking temperature, μ_0 is the permeability of free space, V is volume, M_{S0} is saturation magnetization at room temperature, H_0 is applied field, H_{k0} is microcoercivity at room temperature, t is time, τ_0 is the atomic reorganization time, and $\vartheta(T) \stackrel{\text{def}}{=} \frac{M_S(T)}{M_{S0}}$. The second term in brackets reduces to 1 for small H_0. The first term in brackets reduces to a set of constant C_iM_{S0} for predetermined volumes, V_i. The equation then simplifies to

$$\frac{T_{Bi}}{\vartheta^2(T_{Bi})} = C_iM_{S0}. \quad (2)$$

For each temperature step, T_i, a new T_c is found, and blocking temperatures are recalculated using equation (2). Any grains that have a new $T_b < T_i$ are assumed to be unblocked, and grains with $T_b > T_i$ remain blocked.

To simulate multidomain behavior where $T_b \neq T_{ub}$, we use the phenomenological model of *Fabian* [2000] which was applied to paleointensity experiments in *Fabian* [2001] and modified by *Leonhardt et al*. [2004] to include the effects of partial thermal remanent magnetization (pTRM) tails. A complete description can be found in these papers, and we briefly summarize it here.

Remanent magnetization at room temperature (T_0) acquired in a weak field, *H*, can be described by:

$$M(T_0)=M_S(T_0)\int\int_{T_0}^{T_C} H_{eff}(T_b,T_{ub})\chi(T_b,T_{ub})dT_{ub}dT_b \tag{3}$$

where

$$H_{eff}(T_b,T_{ub})=H(T_b,T_{ub})+\alpha M(T_b,T_{ub}). \tag{4}$$

α is a magnetostatic interaction coefficient which *Fabian* [2001] determines to have a negligible effect on paleointensity experiments and we therefore set to zero. The field function, $H(T_b,T_{ub})$, describes the field history (supporting information Figure S3). In the most straightforward case of thermal demagnetization by cooling from T_i in zero-field, $H(T_b,T_{ub})$ is zero for all $T_{ub} < T_i$ (supporting information Figure S3b). During acquisition of a pTRM acquired by cooling from $T_i < T_c$ to T_0 in field *H*, $H(T_b,T_{ub}) = H$ in the region where both $T_b < T_i$ and $T_{ub} < T_i$ (supporting information Figure S3c). This type of pTRM is referred to as pTRM* [*Fabian*, 2001; *Leonhardt et al*., 2004] and is distinguished from pTRM acquired on cooling from $T_i > T_c$.

The field function is convolved with the characteristic function $\chi(T_b,T_{ub})$. The form of $\chi(T_b,T_{ub})$ used by both *Fabian* [2001] and *Leonhardt et al*. [2004] is based on the Cauchy-function:

$$\varphi(x,s) \equiv \frac{1}{1+(x/s)^2} \tag{5}$$

We follow the specific formulation of *Leonhardt et al*. [2004], where

$$\chi(T_b,T_{ub})=\gamma(\tau_b)\varphi(\tau_{ub}-\tau_b,\lambda_i(\tau_b)) \tag{6}$$

$$\lambda_1(\tau)=\alpha_{11}+\alpha_{12}\varphi(\tau-\alpha_{1t},\alpha_{13}) \text{ for } \tau_b < \tau_{ub} \tag{7}$$

$$\lambda_2(\tau)=\alpha_{21}+\alpha_{22}\varphi(\tau-\alpha_{2t},\alpha_{23}) \text{ for } \tau_b \geq \tau_{ub} \tag{8}$$

$$\gamma(\tau_b)=\beta(\tau_b)\int_{\tau_b}^{1}\varphi(\tau_{ub},\lambda_1(\tau_b))d\tau_{ub}+\int_0^{\tau_b}\varphi(\tau_{ub},\lambda_2(\tau_b))d\tau_{ub} \tag{9}$$

$$\beta(\tau_b)=\beta_1+\beta_2\ \varphi(\tau_b-\beta_t,\beta_3) \tag{10}$$

τ is reduced temperature, $(T-T_0)/(T_C-T_0)$. The α_{ij} parameters describe variation in the width of the T_{ub} distribution for constant T_b. A SD population will have a very narrow distribution and an MD population will have a wider distribution. If $\alpha_{i2} = 0$, the width of the unblocking temperature distribution is the same for all τ_b. If $\alpha_{i2} > 0$, the distribution has a constant part α_{i1}, and a variable part with a peak at α_{it} and a width of α_{i3}. The β_k describe the temperature range over which remanence is acquired. Examples of $\chi(T_b,T_{ub})$ functions used are shown in supporting information Figure S4.

As described, this phenomenological model does not explain the experimentally observed pTRM*-tail, whereby a pTRM* acquired on cooling from $T_i < T_c$ is not fully removed by zero field cooling from the same T_i. *Leonhardt et al*. [2004] approximate the effects of a pTRM*-tail by allowing the pTRM*-tail to overprint the NRM at $T_{ub} > T_i$ by a factor of $\tau = 0.1$ (supporting information Figure S3e). This means that for acquisition of a pTRM* acquired by cooling from T_i to T_0, $H(T_b,T_{ub}) = H$ where both $T_b < T_i$ and $T_{ub} < T_i + \tau(T_c-T_0)$. *Leonhardt et al*. [2004] find that $\tau = 0.1$ provides the best agreement between modeled and experimental calculations of pTRM*-tails.

We add to this approach by incorporating the effects of the cation reordering in a manner similar to that described above for the SD case. Integrations are carried out by a numerical summation over a grid with 1°C resolution. In applying the phenomenological model, we modeled an SD, PSD, and MD scenario, following *Leonhardt et al*. [2004]: SD ($\alpha_{11} = \alpha_{21} = 0.001$, $\alpha_{12} = \alpha_{22} = 0$, $\beta_1 = 0$, $\beta_2 = 1$, $\beta_3 = 0.2$, $\beta_t = 0.9$); pseudo-single domain, PSD ($\alpha_{11} = \alpha_{21} = 0.05$, $\alpha_{12} = \alpha_{22} = 0$, $\beta_1 = 0$, $\beta_2 = 1$, $\beta_3 = 0.5$, $\beta_t = 0.9$); MD ($\alpha_{11} = \alpha_{21} = 0.4$,

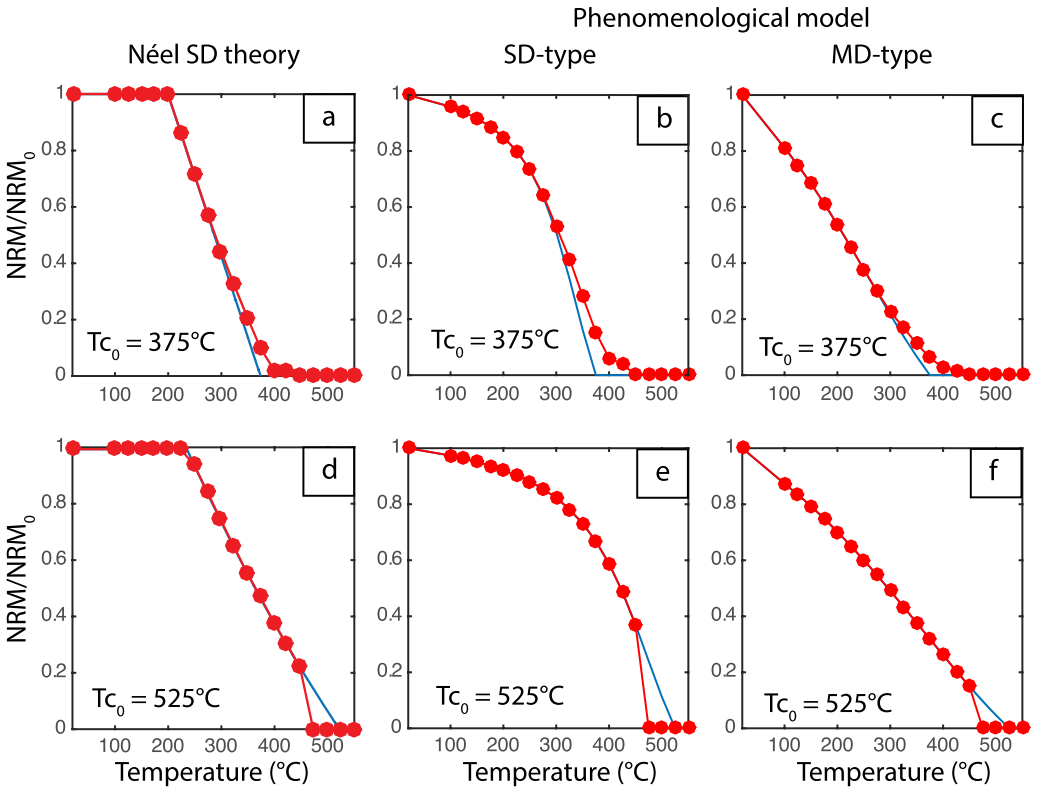

Figure 2. Thermal demagnetization modeling results. Solid blue line represents starting blocking temperature spectrum. Red circles are final result, as measured during demagnetization experiment. (a-c) Starting $T_c = 375°C$. (d-f) Starting $T_c = 525°C$. (a, d) Model based on SD Néel theory, with minimum blocking temperature of 200°C. (b, e) Phenomenological model of *Fabian* [2000], SD-type: $\alpha_{11}=\alpha_{21}=0.001$, $\alpha_{12}=\alpha_{22}=0$, $\beta_1=0$, $\beta_2=1$, $\beta_3=0.2$, $\beta_t=0.9$. (c, f) Phenomenological model, MD-type: $\alpha_{11}=\alpha_{21}=0.4$, $\alpha_{12}=\alpha_{22}=0$, $\beta_1=0$, $\beta_2=1$, $\beta_3=0.5$, $\beta_t=0.9$. Insets show starting $\chi(T_b,T_{ub})$ distributions.

$\alpha_{12} = \alpha_{22} = 0$, $\beta_1 = 0$, $\beta_2 = 1$, $\beta_3 = 0.5$, $\beta_t = 0.9$). The $\chi(T_b,T_{ub})$ distributions for these three cases are shown in supporting information Figure S4. PSD results are not shown. In all cases they are intermediary between the SD and MD cases.

We apply the Néel and phenomenological models to both basic thermal demagnetization experiments and paleointensity experiments. For the paleointensity experiments, we present results for the IZZI (in-field – zero-field, zero-field – in-field) protocol [*Tauxe and Staudigel*, 2004; *Yu et al.*, 2004], which alternates the order in which the in-field and zero-field treatments are applied in order to highlight behavior arising from nonreciprocity of pTRM*. pTRM checks [*Coe*, 1967] are carried out during the ZI steps, following the zero-field measurement. Modeled laboratory heating starts at 100°C and proceeds in 25°C steps to 600°C. It is assumed that during each temperature step 1 h is spent at T_i, and we neglect time spent ramping temperature up and down. We allowed the laboratory field (H_{lab}) to be either parallel or perpendicular to the NRM, and in all cases let the ancient field (H_{anc}) be equal to H_{lab}, so that the ideal slope of all pTRM-NRM (Arai) plots should be 1. We show results from three cases: (1) the remanence is carried by a single, relatively disordered phase which has a starting $T_{c0} = 375°C$; (2) the remanence is carried by a single, relatively ordered phase which has a starting $T_{c0} = 525°C$; and (3), the remanence is carried by two phases, 75% by a disordered phase with $T_{c0} = 375°C$, and 25% by an oxyexsolved phase with $T_c = 580°C$ and which does not undergo cation reordering.

4. Results

4.1. Thermal Demagnetization

When we apply the models to thermal demagnetization, we find that for rapidly cooled samples with $T_{c0} < T_{close}$, the measured unblocking temperature distribution has a high-temperature tail that is not present in the sample prior to laboratory heating (Figures 2a–2c). This is induced during laboratory heating

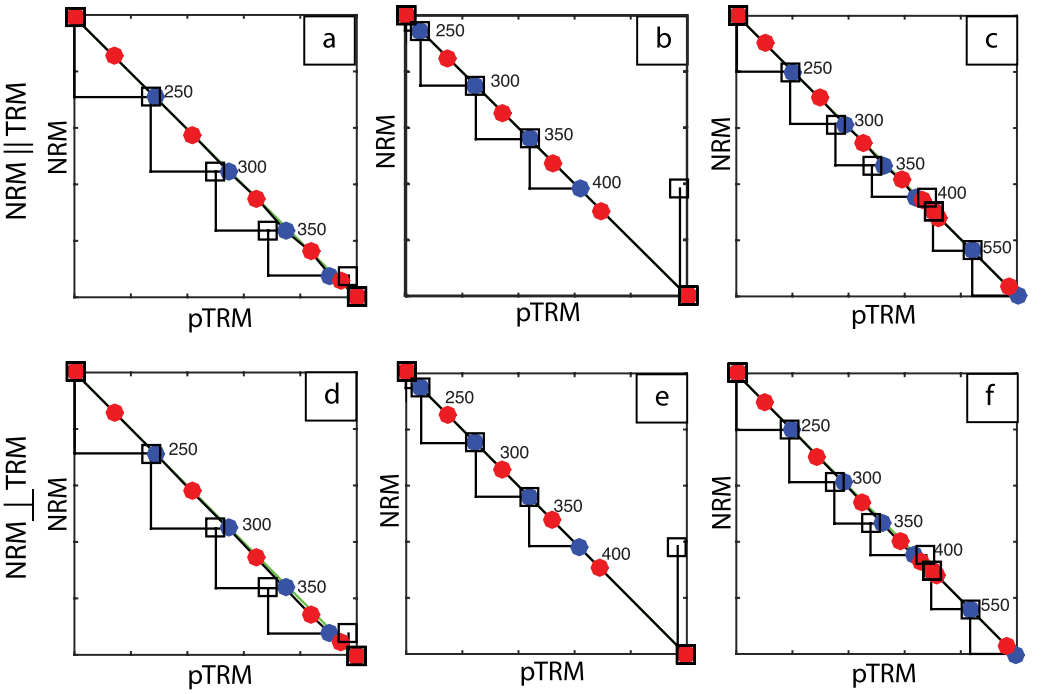

Figure 3. Single-domain paleointensity modeling results using Neel theory. All experiments follow the IZZI protocol: blue symbols are zero-field first (ZI), red symbols are in-field first (IZ). Squares are pTRM checks. $T_{b\text{-}min} = 200°C$. Green line is ideal slope of −1. (a-c) NRM is parallel to applied field. (d-f) NRM is orthogonal to applied field. (a, d) Single reordering phase with starting $T_{c0} = 375°C$. (b, e) Single reordering phase with starting $T_{c0} = 525°C$. (c, f) Two-phase: one reordering phase with starting $T_{c0} = 375°C$ (70% of NRM), and one nonreordering phase that unblocks between 520 and 580°C.

and should be identified by unblocking temperatures higher than T_c. (Because the total amount of time at elevated temperature is much less during T_c measurement than during thermal demagnetization, it is usually possible to accurately measure T_c without inducing significant reordering at $T < T_c$.)

By contrast, slowly cooled samples with $T_{c0} > T_{close}$ have a measured blocking temperature spectrum that is truncated with respect to the distribution prior to laboratory heating (Figures 2d–2f). This arises because for $T > T_{close}$, T_c is "reset" to 375°C and any remaining remanence is immediately wiped out.

4.2. Paleointensity Experiments

In the paleointensity experiments, the results are more complicated. For the purely SD case, modeled results using Néel theory and using the phenomenological model are nearly identical, and we show only the Néel results in Figure 3. Deviations from the ideal Arai slope are slight, but pTRM checks fail when significant unblocking occurs in temperature intervals where cation reordering is also taking place (Figure 3). For $T < T_{close}$, T_c and T_b increase with progressive heating. This means that the pTRM* acquired during the pTRM check will be less than the original pTRM* acquired at the same temperature. This type of pTRM check failure is largest where the sample starts out in a relatively disordered state with $T_{c0} = 375°C$ and significant variations in T_c happen at $T < T_{close}$ (e.g., Figures 3a, 3d, 3c, and 3f). For the first temperature step at $T > T_{close}$, the pTRM check deviates in the opposite sense: more pTRM* is acquired during the pTRM check than during the original pTRM*. Because T_c is rapidly reset to 375°C on heating above T_{close}, blocking temperatures are relatively lower with respect to the laboratory heating temperature and more pTRM* may be acquired. This type of failure is largest where T_{c0} is 525°C and the sample is in a relatively stable and ordered state until the laboratory temperature exceeds T_{close} (Figures 3b and 3e).

While the pTRM check deviations are identical in the parallel and orthogonal cases, the deviations from the ideal slope differ for these two cases. When the NRM is parallel to H_{lab}, all of the IZ steps fall exactly on the ideal slope line. By contrast, the ZI steps fall below the line, leading to a slight zig-zag behavior in the temperature interval where significant cation reordering is taking place (Figure 3a). During the ZI steps, less pTRM* is gained compared to the amount of NRM lost, because of the increase in (un)blocking

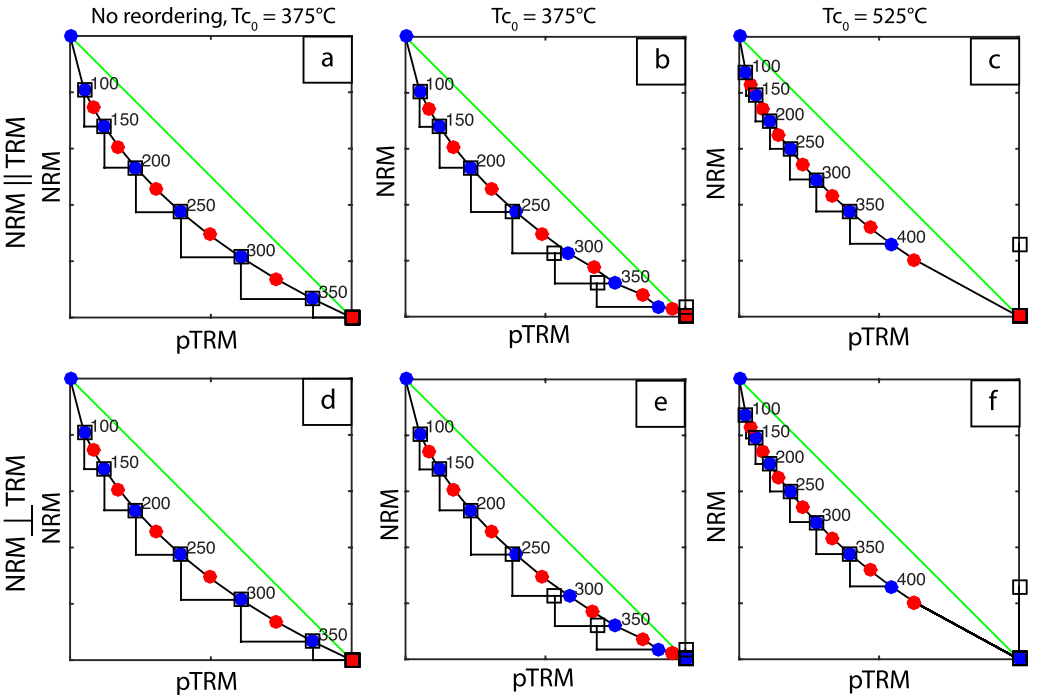

Figure 4. Multidomain paleointensity modeling results. Symbols as in Figure 3. (a-c) NRM parallel to applied field. (d-f) NRM orthogonal to applied field. (a, d) No reordering and starting $T_{c0} = 375°C$. (b, e) Reordering incorporated and starting $T_{c0} = 375°C$. (c, f) Reordering incorporated and starting $T_{c0} = 525°C$.

temperatures between the two steps. The opposite is true during the IZ steps; not all of the pTRM* acquired is removed by the subsequent zero-field step. However, because the NRM and H_{lab} are in the same direction and of equal magnitude, the technique cannot distinguish between NRM and pTRM*. We note that if one were to perform a standard Coe-type paleointensity experiment where the zero-field step is always performed first, the Arai plot would be slightly concave up (sagging below the ideal slope) in the cation-reordering temperature interval. When NRM is perpendicular to H_{lab}, both IZ and ZI steps fall below the ideal slope (Figure 3d). This deviation is slightly less for the IZ case which can lead to a slight zig-zag depending on how much reordering takes place in a given temperature interval.

Results for the MD case are shown in Figure 4 without pTRM*-tails and in Figure 5 incorporating pTRM*-tails. Figures 4a and 4d show the results for the parallel and perpendicular case where $T_c = 375°C$, but no cation reordering is incorporated. There is no difference between the two cases, and the results demonstrate the concave-up behavior that has been experimentally observed and is predicted by the phenomenological model [*Fabian*, 2001] due to the nonreciprocity of pTRM*. Figures 4b, 4c, 4e, and 4f incorporate cation reordering and the results are essentially analogous those documented for the SD case, but any deviations are no longer with respect to the ideal slope of 1, but with respect to the nonreordering case.

When we incorporate pTRM*-tails and before we consider the effects of cation reordering we see in the parallel case (Figure 5a) that the pTRM* acquired during the pTRM check is greater than that acquired during the original pTRM* (as shown by *Leonhardt et al.* [2004]). This is true to a much lesser degree in the orthogonal case (Figure 5d), but now a pronounced zig-zag effect is induced whereby the ZI steps fall closer to the ideal slope than the IZ steps. This zig-zag behavior for the IZZI protocol is predicted by *Yu et al.* [2004] using a different mathematical formulation of MD remanence behavior, and has also been experimentally observed [*Yu and Tauxe*, 2005].

When we consider the additional effects of cation reordering, we see no deviation from the nonreordering cases in temperature intervals where little cation reordering takes place. However, for intervals where significant reordering takes place, and for $T < T_{close}$, the pTRM checks shift toward the left in the Arai plot, compared to the nonreordering case (Figures 5b and 5e). In the parallel case (Figure 5b), this has the effect of causing some of the pTRM checks to seemingly "pass," when in fact the coincidence of the two pTRM*'s

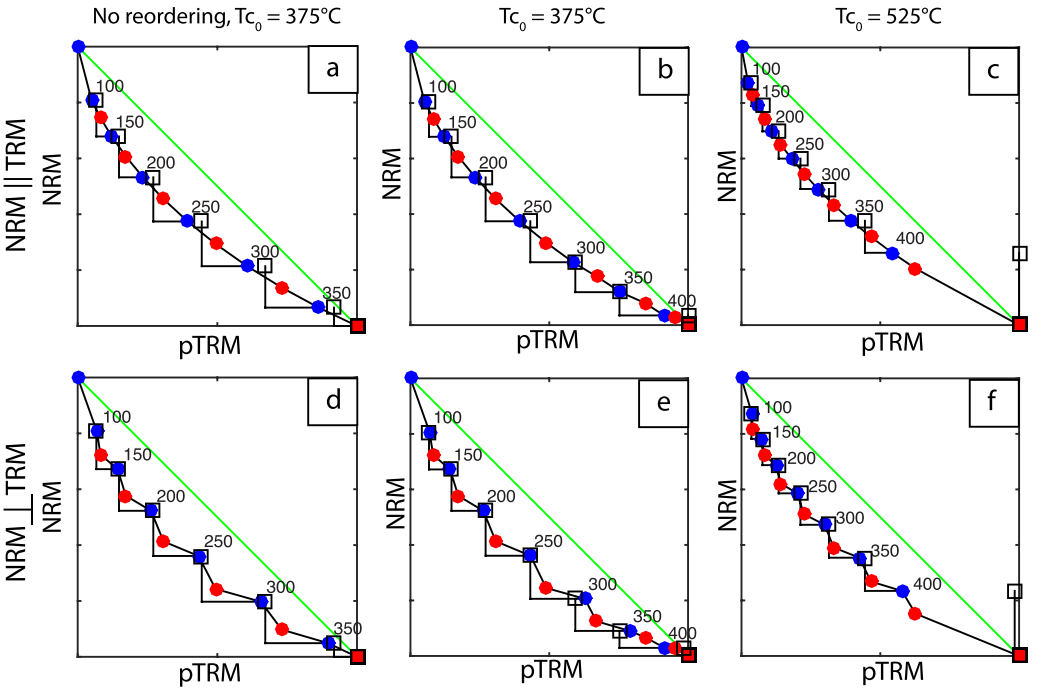

Figure 5. Multidomain paleointensity modeling results incorporating pTRM tail effect. Symbols as in Figure 3. (a-c) NRM parallel to applied field. (d-f) NRM orthogonal to applied field. (a, d) No reordering and starting T_{c0} = 375°C. (b, e) Reordering incorporated and starting T_{c0} = 375°C. (c, f) Reordering incorporated and starting T_{c0} = 525°C.

results from two separate effects (pTRM*-tails and cation reordering) that have opposite results and cancel each other out. In the orthogonal case (Figure 5f), the pTRM checks in this same temperature interval now appear to "fail" because they were less divergent to start with.

5. Discussion

For samples that contain homogeneous titanomagnetite with moderate degrees of titanium substitution (*x* approximately 0.2 – 0.5), the sample's thermal history will play a large role in determining the Curie and unblocking temperature distribution that carries the NRM. Slowly cooled samples will have higher Curie and unblocking temperatures because of the relatively ordered state of the titanomagnetite. By contrast, rapidly cooled samples will have lower Curie and unblocking temperatures because a high-temperature, disordered state is preserved by quenching.

Modeling results demonstrate that further cation reordering during progressive thermal demagnetization makes it impossible to accurately measure the unblocking temperature spectrum. Although deviations from the starting T_{ub} spectrum are relatively small, they could lead to misinterpretation of results, especially in cases where T_{ub} may be linked to paleotemperature [e.g., *Dunlop et al*., 1997b, 1997a; *McClelland et al*., 2004; *McClelland-Brown*, 1981; *Middleton and Schmidt*, 1982; *Paterson et al*., 2010]. The apparent high-temperature "tail" induced where T_{c0} is close to the quenched state may be interpreted as arising from an MD contribution or from a second phase with a distinct T_c. In theory, this "reordering tail" can be identified by unblocking temperatures higher than T_c, but in practice this may be complicated by the actual presence of multiple phases.

In the case of the paleointensity experiments, the zig-zag and/or concave up behavior that arises from cation reordering (Figure 3) could be mistaken for similar behavior produced by nonreciprocity in MD grains. However, the reordering effects are slight, and in practice most likely would not be distinguished from other sources of noise.

The effects on pTRM checks are much more pronounced. In the SD case, the apparent failure of pTRM checks could lead to rejection of results that are actually correct. For the MD case modeled here, the MD

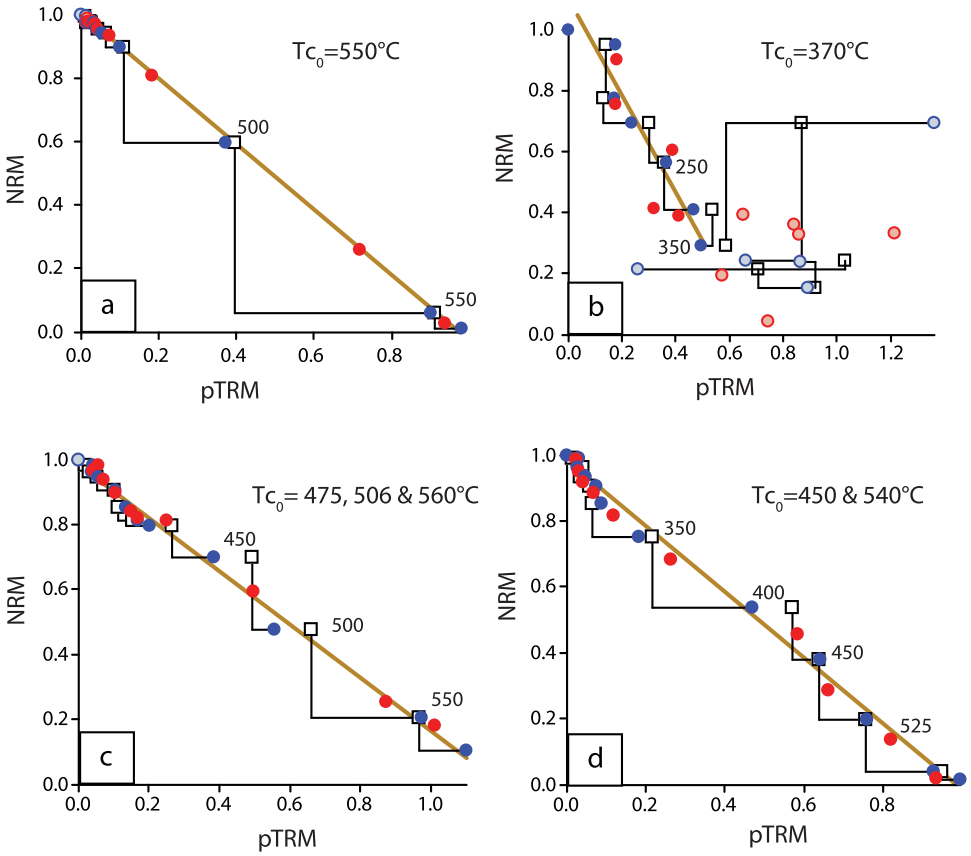

Figure 6. IZZI-style paleointensity results from the Mt. St. Helens 1980 pyroclastic deposits. Data from *Bowles et al.* [2015]. (a) Specimen MSH003-G3z1. NRM carried by oxyexsolved titanomagnetite. (b) Specimen MSH008-Jz2. NRM carried by homogeneous, MD titanomagnetite. (c) Specimen MSH007-D2z1 and (d) specimen MSH012-N4z1; NRM carried by both homogeneous and oxyexsolved titanomagnetite. All specimens show an increase in unstable behavior in the temperature region over which the homogeneous titanomagnetite undergoes significant reordering (~350 - 500°C).

behavior is so extreme that none of Arai plots shown would likely be allowed to "pass." It may be possible to interpret the sense in which pTRM checks fail in terms of the process causing the failure. Nonreciprocity of pTRM* and cation reordering have opposite effects for $T < T_{close}$, but the relative magnitude of each will depend on the shape of the $\chi(T_b,T_{ub})$ function; the angle of H_{lab} with respect to the NRM; the starting T_{c0}; and the relative temperature intervals over which remanence is lost and over which cation reordering takes place.

What is clear is that "failure" of pTRM checks is not necessarily a sign of chemical alteration, but may reflect a change in the capacity for remanence acquisition that is independent of chemical alteration. In all cases, the magnitude of the observed effect depends on what fraction of the remanence unblocks in the affected temperature region.

IZZI-style paleointensity results from the Mt. St. Helens 1980 deposits are described in *Bowles et al.* [2015]. Comparison of the models with these data (Figure 6) shows some similarities, but also significant differences, as we describe below. The samples contain variable proportions of homogeneous MD titanomagnetite with Curie temperatures between 350 and 500°C and PSD oxyexsolved titanomagnetite with $T_c \geq 540$°C. The homogeneous titanomagnetite has been shown to undergo significant reordering at temperatures between ~300 and 500°C, while the oxyexsolved titanomagnetite does not. Samples that contain only the oxyexsolved titanomagnetite show ideal behavior in the paleointensity experiments (Figure 6a). By contrast, samples dominated by the homogeneous titanomagnetite have univectoral decay up to ~350°C accompanied by a scattered but linear Arai plot (Figure 6b). At $T > 350$°C, sample behavior becomes significantly more unstable, with extremely scattered and unpredictable directions and intensities. The temperature at which samples become unstable coincides with the temperature where the reordering

phenomenon becomes important on laboratory time scales. However, the nonideal behavior is considerably more extreme and less systematic than that predicted by the models.

Samples that contain both fractions display an intermediate behavior (Figures 6c and 6d), where for $T < 300–350°C$ and $T > \sim 500°C$ pTRM checks pass and behavior is relatively ideal. However, in the reordering temperature interval of ~300 to 500°C, behavior is nonideal, with points deviating from linearity and failure of pTRM checks. Again, the deviation from linearity is more erratic than predicted by the model. While pTRM check failure is also a feature of the model, the sense in which the checks fail is opposite to that predicted by the reordering behavior. It may be that the pTRM check failure is instead dominated by the pTRM* tail in these samples. What all the samples have in common, however, is an increase in unstable behavior in the temperature interval over which significant reordering takes place (~300 – 500°C) and more stable behavior at both lower and higher temperatures.

6. Conclusions

We have modeled the effects of T_c variations in titanomagnetite arising from a thermally activated reordering process on standard thermal demagnetization and paleointensity experiments. The results have important implications for the interpretation of many paleomagnetic studies which rely on a titanomagnetite-bearing remanence. Models based on both single-domain Néel theory and a phenomenological model of multidomain behavior show that it is not possible to accurately measure the unblocking temperature spectrum without modifying it. Samples with a starting $T_{c0} < T_{close}$ will develop a high-temperature "tail" and samples with a starting $T_{c0} > T_{close}$ will have their original Tb spectrum truncated at $T \approx T_{close}$. Differences are not large, but could lead to misinterpretation of data. Modeled behavior during paleointensity experiments varies slightly depending on domain state, angle of the laboratory field with respect to the NRM, and the order in which the in-field and zero-field steps are applied during the experiment. However, in most cases relatively small deviations from the ideal slope (or from the nonreordering case) are found. Modeling predicts much larger deviations in the pTRM checks, with the checks shifted to the left (less pTRM* acquired) in the region where significant reordering takes place. This arises from the fact that an increase in Tc during experimental heating leads to a reduction in the capacity for remanence acquisition. Compared to actual, IZZI-style paleointensity results, the modeled deviations are in the same temperature intervals but are more systematic than observed in the actual data. Modeling suggests that a reordering process and attendant Tc changes may be a common contributing factor to failure of paleointensity experiments, although in practice it may be difficult to distinguish this type of failure from other causes of nonideal behavior.

Acknowledgments
This work was supported by National Science Foundation grants EAR-1315971 (to JB) and EAR-1315845 (to MJ). Data underlying the model are shown in the supporting information. Many thanks to reviewers Karl Fabian, Lennart de Groot, and Yongjae Yu who provided helpful feedback that improved this manuscript. In particular we thank Karl for suggesting the order-parameter formulation. This is IRM publication 1609.

References

Bowles, J. A., M. J. Jackson, T. S. Berquó, P. A. Sølheid, and J. S. Gee (2013), Inferred time-and temperature-dependent cation ordering in natural titanomagnetites, *Nat. Commun.*, *4*, 1–9, doi:10.1038/ncomms2938.

Bowles, J. A., J. S. Gee, M. Jackson, and M. S. Avery (2015), Geomagnetic paleointensity in historical pyroclastic density currents: Testing the effects of emplacement temperature and postemplacement alteration, *Geochem. Geophys. Geosyst.*, *16*, 3607–3625, doi:10.1002/2015GC005910.

Coe, R. S. (1967), The determination of paleo-intensities of the Earth's magnetic field with emphasis on mechanisms which could cause non-ideal behavior in Thellier's method, *J. Geomagn. Geoelectr.*, *19*, 157–179.

Dunlop, D., and O. Özdemir (1997), *Rock Magnetism: Fundamentals and Frontiers*, 573 pp., Cambridge Univ. Press, Cambridge, U. K.

Dunlop, D. J., O. Özdemir, and P. W. Schmidt (1997a), Paleomagnetism and paleothermometry of the Sydney Basin 2. Origin of anomalously high unblocking temperatures, *J. Geophys. Res.*, *102*, 27,285–27,295.

Dunlop, D. J., P. W. Schmidt, Ö. Özdemir, and D. A. Clark (1997b), Paleomagnetism and paleothermometry of the Sydney Basin 1. Thermoviscous and chemical overprinting of the Milton Monzonite, *J. Geophys. Res.*, *102*, 27,271–27,283.

Fabian, K. (2000), Acquisition of thermoremanent magnetization in weak magnetic fields, *Geophys. J. Int.*, *142*, 478–486.

Fabian, K. (2001), A theoretical treatment of paleointensity determination experiments on rocks containing pseudo-single or multi domain magnetic particles, *Earth Planet. Sci. Lett.*, *188*, 45–58.

Harrison, R. J., and A. Putnis (1999), The magnetic properties and crystal chemistry of oxide spinel solid solutions, *Surv. Geophys.*, *19*, 461–520.

Jackson, M. J., and J. A. Bowles (2013), Reversible changes in Curie temperature of natural titanomagnetites: Occurrences and experimental observations, Abstract GP53B-1133 presented at 2013 Fall Meeting, AGU, San Francisco, Calif.

Jackson, M. J., and J. A. Bowles (2014), Curie temperatures of titanomagnetite in ignimbrites: Effects of emplacement temperatures, cooling rates, exsolution and cation ordering, *Geochem. Geophys. Geosysyst.*, *15*, 4343–4368, doi:10.1002/2014GC005527.

Lappe, S. C. L. L., J. Bowles, M. Jackson, and D. Keavney (2014), XMCD and Magnetic Evidence for Cation Reordering in Synthetic Mg-and Al-substituted Titanomagnetites, Abstract GP33B-06 presented at 2014 Fall Meeting, AGU, San Francisco, Calif.

Lappe, S. C. L. L., J. A. Bowles, M. J. Jackson, and E. Arenholz (2015), XMCD and XAS examination of cation ordering in synthetic Mg- and Al-substituted titanomagnetites, Abstract GP43A-1237 presented at 2015 Fall Meeting, AGU, San Francisco, Calif.

Leonhardt, R., D. Krása, and R. S. Coe (2004), Multidomain behavior during Thellier paleointensity experiments: A phenomenological model, *Phys. Earth Planet. Inter.*, *147*, 127–140.

McClelland, E., C. J. N. Wilson, and L. Bardot (2004), Palaeotemperature determinations for the 1.8-ka Taupo ignimbrite, New Zealand, and implications for the emplacement history of a high-velocity pyroclastic flow, *Bull. Volcanol.*, *66*, 492–513.

McClelland-Brown, E. (1981), Paleomagnetic estimates of temperatures reached in contact metamorphism, *Geology*, *9*, 112–116.

Middleton, M. F., and P. W. Schmidt (1982), Paleothermometry of the Sydney basin, *J. Geophys. Res.*, *87*, 5351–5359.

Néel, L. (1949), Théorie du trainage magnétique des ferromagnétiques en grains fins avec applications aux terres cuites, *Ann. Geophys.*, *5*, 99–137.

Paterson, G. A., A. P. Roberts, C. Mac Niocaill, A. R. Muxworthy, L. Gurioli, J. G. Viramonté, C. Navarro, and S. Weider (2010), Paleomagnetic determination of emplacement temperatures of pyroclastic deposits: An under-utilized tool, *Bull. Volcanol.*, *72*, 309–330.

Tauxe, L. (2010), *Essentials of Paleomagnetism*, 489 pp., Univ. of Calif. Press, Los Angeles.

Tauxe, L., and H. Staudigel (2004), Strength of the geomagnetic field in the Cretaceous Normal Superchron: New data from submarine basaltic glass of the Troodos Ophiolite, *Geochem. Geophys. Geosyst.*, *5*, Q02H06, doi:10.1029/2003GC000635.

Yu, Y., and L. Tauxe (2005), Testing the IZZI protocol of geomagnetic field intensity determination, *Geochem. Geophys. Geosyst.*, *6*, Q05H17, doi:10.1029/2004GC000840.

Yu, Y., L. Tauxe, and A. S. Genevey (2004), Toward an optimal geomagnetic field intensity determination technique, *Geochem. Geophys. Geosyst.*, *5*, Q02H07, doi:10.1029/2003GC000630.

Geochemistry, Geophysics, Geosystems

Supporting Information for

Effects of titanomagnetite reordering processes on thermal demagnetization and paleointensity experiments

J.A. Bowles[1] and M.J. Jackson[2]

[1]Department of Geosciences, University of Wisconsin – Milwaukee, Milwaukee, WI, USA
[2] Institute for Rock Magnetism, University of Minnesota, Minneapolis, MN, USA

Contents of this file

Introduction

This supporting information provides one figure that illustrates the data underlying our models; one figure that illustrates the functional form of an assumed saturation magnetization function; and two figures that illustrate the functional forms incorporated in the phenomenological modeling.

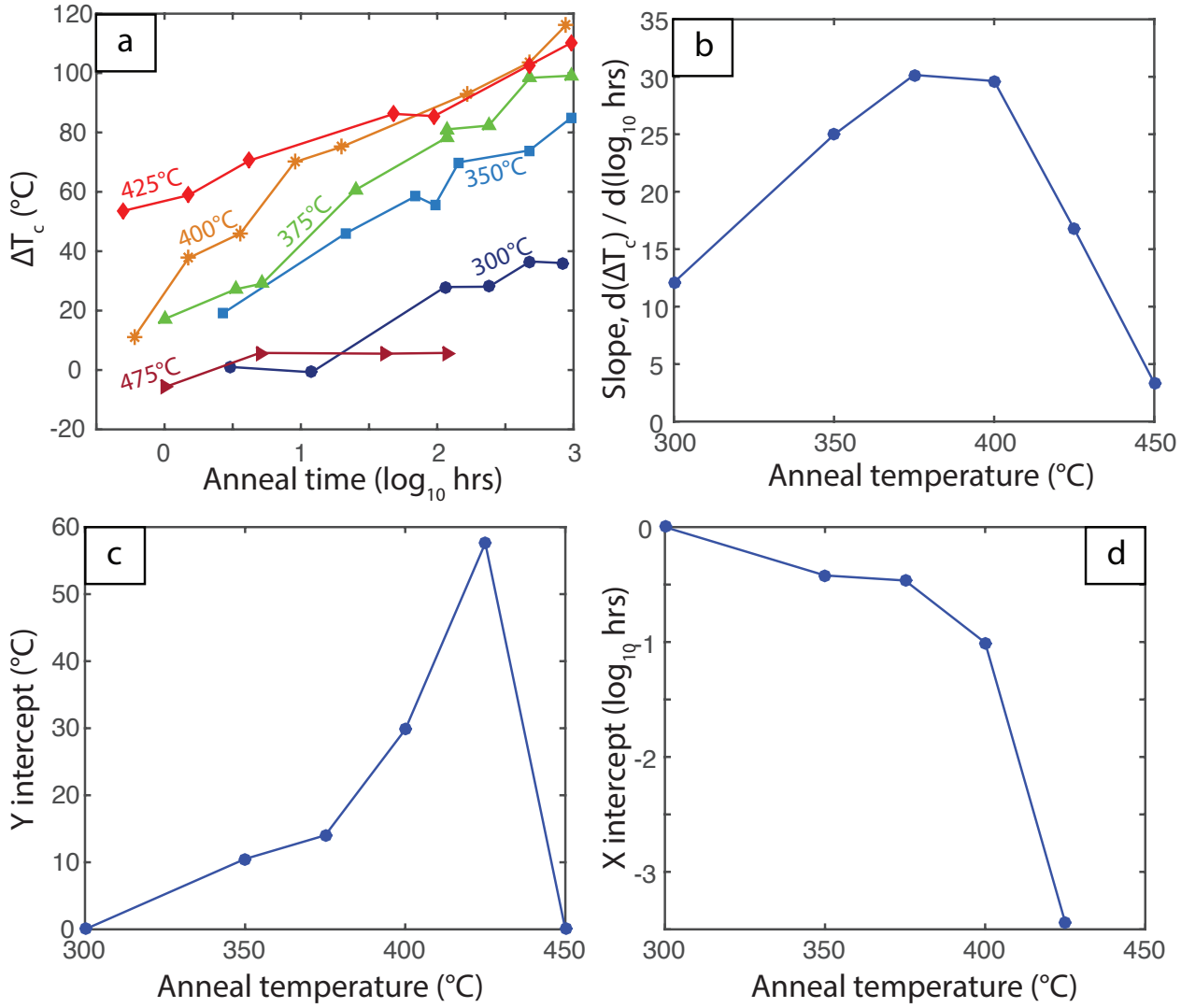

Figure S1. Isothermal anneal results from sample MSH008 used in modeling. (a) Increase in T_c vs $\log_{10}$ anneal time for isothermal annealing at 300°C (dark blue circles); 350°C (light blue squares); 375°C (green triangles); 400°C (yellow stars); 425°C (light red triangles); and 450°C (dark red sideways triangles). (b) Best-fit slope to data from (a) as a function of temperature. Fits at 300°C and 450°C forced to zero Y intercept. These slopes represent the change in T_c per unit time under isothermal conditions. (c) Y-intercept used in modeling. (d) X-intercept which may be thought of as an activation time for the process.

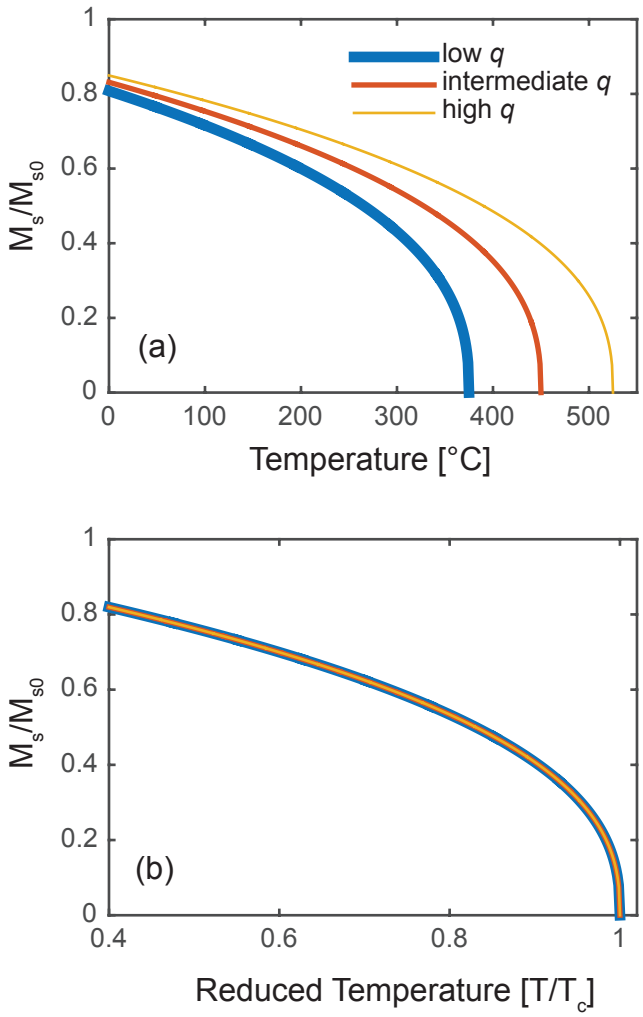

Figure S2. Variations in $M_s(T,q)$ used in modeling. As described in the main text, we use the formulation $M_s(T,q) = M_{s0}[1-T/T_c(q)]^{\gamma}$, where $M_{s0} = M_s$ at 0 K (absolute zero), q is the order parameter, and $\gamma = 0.39$. Because T_c is a function of q, $M_s(T,q)$ necessarily varies with q (a). However, as a function of reduced temperature, $M_s(T/T_c(q))$ is constant (b).

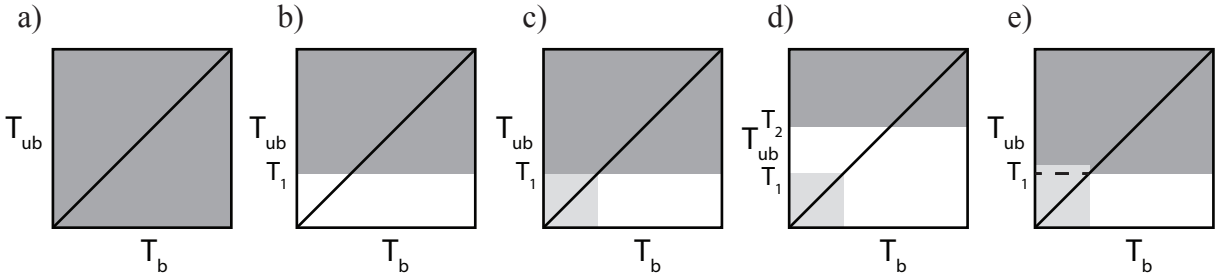

Figure S3. Representations of the field function, $H(T_b, T_{ub})$, used in modeling. (a) Starting magnetization is assumed to be a total TRM acquired in H_{anc}, represented by dark gray. (b) After zero-field heating to T_1, magnetization for all $T_{ub} < T_1$ is removed. (c) A pTRM* is acquired after heating in a laboratory field H_{lab} (light gray). (d) pTRM* acquired during a pTRM check at T_1 following zero-field heating to T_2. (3) pTRM* acquired after heating to T1, including pTRM* tail of $\tau \times (T_c - T_0)$.

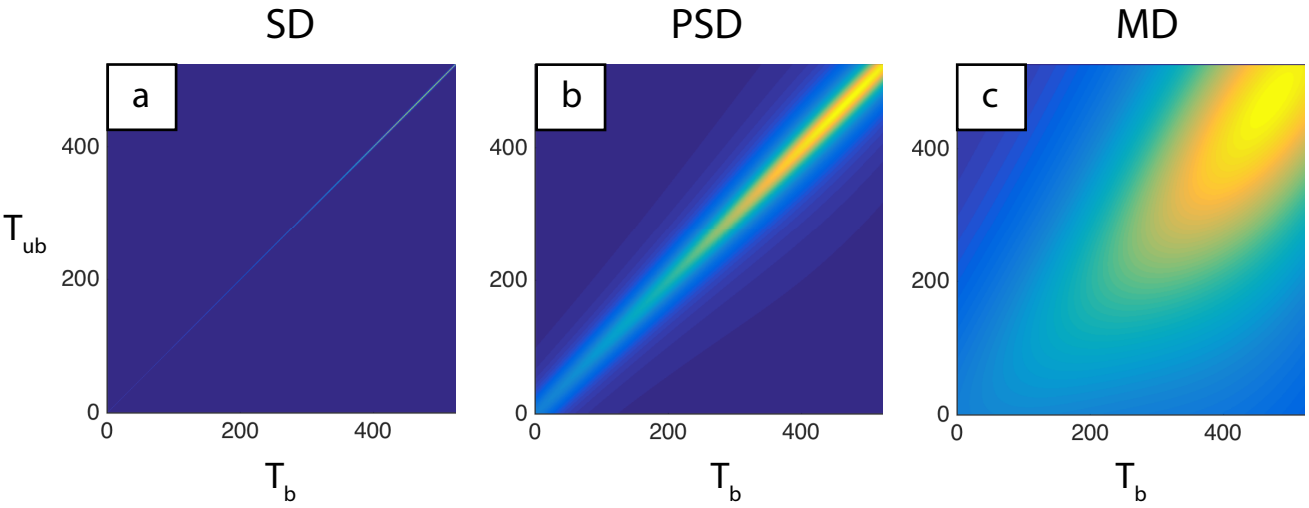

Figure S4. Susceptibility functions, $X(T_b, T_{ub})$, used in phenomenolgical modeling following Fabian [2001] and Leonhardt et al. [2004]. In all cases shown here, $T_c = 525°C$. (a) Single-domain, SD, case: $\alpha_{11} = \alpha_{21} = 0.001$, $\alpha_{12} = \alpha_{22} = 0$, $\beta_1 = 0$, $\beta_2 = 1$, $\beta_3 = 0.2$, $\beta_t = 0.9$). (b) Pseudo-single domain, PSD, case: $\alpha_{11} = \alpha_{21} = 0.05$, $\alpha_{12} = \alpha_{22} = 0$, $\beta_1 = 0$, $\beta_2 = 1$, $\beta_3 = 0.5$, $\beta_t = 0.9$). (c) Multi-domain, MD, case: $\alpha_{11} = \alpha_{21} = 0.4$, $\alpha_{12} = \alpha_{22} = 0$, $\beta_1 = 0$, $\beta_2 = 1$, $\beta_3 = 0.5$, $\beta_t = 0.9$.